Measuring the black hole masses of high redshift quasars

R.J. McLure[1] and M.J. Jarvis[2]

[1] *Institute for Astronomy, University of Edinburgh, Royal Observatory, Edinburgh EH9 3HJ.*
[2] *Sterrewacht Leiden, Postbus 9513, 2300 RA Leiden, the Netherlands*

arXiv:astro-ph/0204473v2 19 Jul 2002

ABSTRACT
A new technique is presented for determining the black-hole masses of high-redshift quasars from optical spectroscopy. The new method utilizes the full-width half maximum (FWHM) of the low-ionization MgII emission line and the correlation between broad-line region (BLR) radius and continuum luminosity at 3000Å. Using archival UV spectra it is found that the correlation between BLR radius and 3000Å luminosity is tighter than the established correlation with 5100Å luminosity. Furthermore, it is found that the correlation between BLR radius and 3000Å continuum luminosity is consistent with a relation of the form $R_{BLR} \propto \lambda L_\lambda^{0.5}$, as expected for a constant ionization parameter. Using a sample of objects with broad-line radii determined from reverberation mapping it is shown that the FWHM of Mg II and Hβ are consistent with following an exact one-to-one relation, as expected if both Hβ and MgII are emitted at the same radius from the central ionizing source. The resulting virial black-hole mass estimator based on rest-frame UV observables is shown to reproduce black-hole mass measurements based on reverberation mapping to within a factor of 2.5 (1σ). Finally, the new UV black-hole mass estimator is shown to produce identical results to the established optical (Hβ) estimator when applied to 128 intermediate-redshift ($0.3 < z < 0.9$) quasars drawn from the Large Bright Quasar Survey and the radio-selected Molonglo quasar sample. We therefore conclude that the new UV virial black-hole mass estimator can be reliably used to estimate the black-hole masses of quasars from $z \sim 0.25$ through to the peak epoch of quasar activity at $z \sim 2.5$ via optical spectroscopy alone.

Key words: galaxies: fundamental parameters – galaxies: active – galaxies: nuclei – galaxies: high redshift – quasars: general – quasars: emission lines

1 INTRODUCTION

A reliable method for estimating the black-hole masses of high-redshift quasars would provide crucial new information for understanding the nature and cosmological evolution of quasars. In this paper we address this problem by deriving a virial black-hole mass estimator based on rest-frame UV observables which is capable of producing reliable quasar black-hole mass estimates from optical spectra out to redshifts of $z \sim 2.5$.

Currently, the most direct measurements of the central black-hole masses of powerful active galactic nuclei (AGN) come from the reverberation mapping studies of 17 Seyferts and 17 PG quasars by Wandel, Peterson & Malkan (1999) and Kaspi et al. (2000) respectively. By measuring the time-lag between the variations of the AGN continuum and the broad Hβ (4861 Å) emission line, these long-term monitoring programmes have delivered direct measurements of the radius of the Hβ emission region from the central ionizing

source ($R_{BLR} = c\tau$, where τ is the time lag between the continuum and Hβ variations). By combining these measurements with the assumption that the FWHM of the Hβ line reflects the virialized bulk motion of the line-emitting material, it is then possible to produce the so-called virial estimate of the central black hole mass (see Wandel, Peterson & Malkan 1999 for a full discussion). Although the virial mass estimate is potentially subject to many uncertainties (eg. Krolik 2001), comparison with the predictions of the completely independent relation between black-hole mass and host-galaxy stellar velocity dispersion have shown the two to be in excellent agreement (Ferrarese et al. 2001, Gebhardt et al. 2000).

Unfortunately, because of the many years of monitoring required, it is unrealistic to expect that reverberation mapping measurements can be obtained for large samples of quasars, even at low redshift. However, the existing reverberation mapping of low redshift AGN has revealed a corre-

lation between R_{BLR} and the monochromatic AGN continuum luminosity at 5100Å (eg. $R_{BLR} \propto \lambda L_{5100}^{0.7}$; Kaspi et al. 2000). By exploiting this correlation to estimate R_{BLR} it is possible to produce a virial black-hole mass estimate from a single spectrum covering the Hβ emission line.

This technique has recently been widely employed to investigate how the masses of quasar black holes relate to the properties of the surrounding host galaxies (eg. McLure & Dunlop 2002;2001; Laor 2001) and the radio luminosity of the central engine (Dunlop et al. 2002; Lacy et al. 2001). However, because of the atmospheric restrictions and relative observational expense of near-infrared spectroscopy, the vast majority of previous studies have relied on optical spectroscopy of the Hβ region. Unfortunately, this effectively enforces a redshift upper limit of $z \simeq 0.8 - 0.9$, with the vast majority of studies concentrating on samples at $z \le 0.3$.

An ideal solution to this problem would be to calibrate a rest-frame UV emission line and continuum measurement such that it becomes possible to produce a virial black-hole mass estimate for high-redshift quasars from relatively straightforward optical spectroscopy. It is the purpose of this paper to provide the required UV calibration. There are two strong, permitted, broad UV lines which are candidates to replace Hβ in the virial black-hole mass estimate; CIV(1549Å) and Mg II(2798Å). We note here that Vestergaard (2002) recently derived a UV virial black-hole mass estimator using the CIV FWHM and the continuum luminosity at 1350Å . Although CIV does have the advantage of being accessible with optical spectroscopy at the very highest redshifts ($3 < z < 5$), where MgII is redshifted into the near-infrared, there are a number of reasons to believe that MgII represents a better substitute for Hβ over the redshift range $0.8 < z < 2.5$.

The main reason for adopting MgII as the UV tracer of BLR velocity is that, like Hβ, MgII is a low-ionization line. Furthermore, due to the similarity of their ionization potentials, it is reasonable to expect that the MgII and Hβ emission lines are produced by gas at virtually the same radius from the central ionizing source, an assumption which is supported by the good agreement between the MgII and Hβ FWHM (see Section 5). This has two important consequences. Firstly, it allows us to directly adopt the reverberation mapping determinations of R_{BLR} when calibrating the correlation between R_{BLR} and 3000Å continuum luminosity. Secondly, because the line-widths of MgII and Hβ should trace the same BLR velocities, we are able to simply substitute the FWHM of MgII for that of Hβ in the virial mass estimator.

There is one further practical advantage which favours MgII over CIV as the UV substitute for Hβ . Due to the fact that MgII becomes accessible to optical spectroscopy at $z \sim 0.3$, both Hβ and MgII can be observed in a single optical spectrum within the redshift interval $0.3 \le z \le 0.9$. Consequently, it is therefore possible to directly compare the results of the new UV virial mass estimator against those of the established optical virial mass estimator for objects at intermediate redshifts. This test is performed in Section 7 using data for the Large Bright Quasar Survey (Forster et al. 2001) and the radio-selected Molonglo quasar sample (Baker et al. 1999).

The structure of this paper can be summarized as follows. In Section 2 we briefly review the main aspects of

the virial black-hole mass estimate, before proceeding in Section 3 to describe the properties of the sample of low-redshift AGN with reverberation mapping results. In Sections 4 and 5 this sample is used to calibrate the relation between broad-line radius and 3000Å continuum luminosity ($R_{BLR} - \lambda L_{3000}$) and to demonstrate the viability of adopting MgII as a direct substitute for Hβ in the virial black-hole mass estimator. Our final calibration of the UV black-hole mass estimator is presented in Section 6. In Section 7 the effectiveness of the new UV black-hole mass estimator is demonstrated by application to members of the Large Bright Quasar Survey (LBQS) and the Molonglo quasar sample (MQS) for which both Hβ and MgII FWHM measurements are available. Our conclusions are presented in Section 8. All cosmological calculations presented in this paper assume $\Omega_m = 0.3, \Lambda = 0.7, H_0 = 70$ kms^{-1}Mpc^{-1}.

2 THE VIRIAL BLACK-HOLE MASS ESTIMATE

The underlying assumption behind the method of estimating AGN black-hole masses from the width of their broad emission lines is that the motion of the line-emitting material is virialized. Under this assumption the width of the broad lines can be used to trace the Keplerian velocity of the broad-line gas, and thereby allow an estimate of the central black-hole mass via the formula :

$$M_{bh} = G^{-1} R_{BLR} V_{BLR}^2 \qquad (1)$$

where R_{BLR} is the BLR radius and V_{BLR} is the Keplerian velocity of the BLR gas. Recent evidence to support the Keplerian interpretation of AGN broad-line widths has been presented by Peterson & Wandel (2000) and Onken & Peterson (2002). These authors demonstrate, at least for several Seyfert galaxies which have been well studied for reverberation mapping purposes, that the FWHM of various emission lines follow the $V_{BLR} \propto R_{BLR}^{-0.5}$ relation expected for Keplerian motion. It is important to note that it is not clear that the virial condition is satisfied for the high-ionization CIV emission line. Substantial evidence exists in the literature that CIV may be produced in some form of outflow, as is suggested by the systematic blue-shift of CIV compared to Hβ (eg. Marziani et al. 1996).

2.1 Broad-line region geometry

In Eqn 1 the velocity of the BLR gas is taken as $V_{BLR} = f \times H\beta(\text{FWHM})$, where f is a geometric factor which relates the Hβ FWHM to the intrinsic Keplerian velocity. Due to the fact that there is currently no consensus on the geometry of the BLR in radio-quiet quasars it is conventional to set $f = \sqrt{3}/2$. However, it is clear that if AGN broad lines are in general produced in a more disc-like configuration, evidence for which has been found in radio-loud quasars by numerous authors (eg. Wills & Browne 1986; Brotherton 1996; Vestergaard, Wilkes & Barthel 2000), then f will be inclination dependent. Indeed, in McLure & Dunlop (2002) evidence was presented that the Hβ FWHM is inclination dependent in radio-quiet quasars, and more consistent with the orbits of the Hβ emitting material having

a flattened disc-like geometry than being randomly orientated. However, even in the scenario where the FWHM of Hβ and MgII are entirely orientation dependent, inclination will only have a significant effect on the virial black-hole mass estimate for those objects within $\sim 15°$ of the line of sight. If quasars are taken to be distributed randomly within $\sim 45°$ of the line of sight (Barthel 1989) then this will only effect some 10% of objects. Consequently, for the purposes of providing a generally applicable UV black-hole mass estimator we adopt $f = 1$ throughout this paper.

3   THE REVERBERATION MAPPED SAMPLE

As mentioned previously, the sample of 17 Seyferts and 17 PG quasars with reverberation mapping measurements (hereafter the RM sample) currently represents the best available set of black-hole mass estimates of powerful broadline AGN. Therefore, it is the objects from this sample which we will use to calibrate the new UV virial black-hole mass estimator. Optical and UV data for the combined 34-object RM sample are listed in Table 1. The R_{BLR} data are taken from Kaspi et al. (2000), with the exception of NGC 4051 for which we take the updated figure of $R_{BLR} = 5.9$ light-days from Peterson et al. (2000).

3.1   Optical data

The 5100Å luminosities for the PG quasars have been calculated using the fluxes from the spectrophotometric study of Neugebauer et al. (1987). For the Seyfert galaxies the 5100Å luminosities are from Kaspi et al. (2000) after conversion to our cosmology. The Hβ FWHM values for the PG quasars are taken from Boroson & Green (1992). The Hβ FWHM values for the Seyfert galaxies are drawn from a number of literature sources which are listed in the caption to Table 1.

3.2   UV data

As with the optical continuum luminosities, the 3000Å luminosities listed in Table 1 for the PG quasars are derived from Neugebauer et al. (1987). In contrast, the 3000Å luminosities for the Seyfert galaxies, together with 17/22 of the MgII FWHM values, are new measurements based on our fitting of spectra from the International Ultraviolet Explorer (IUE) final data archive. A full discussion of our line-fitting method will be presented in a follow-up paper (McLure et al. 2002, in prep). In brief, we fit the region spanning the MgII emission line (2300Å$\rightarrow$ 3100Å) with a combination of a power-law continuum, a FeII emission template and two gaussians representing the broad and narrow components of the MgII emission line.

As with the Hβ emission line, it is crucial to account for blending with broad FeII emission in order to obtain a reliable measurement of the MgII line-width. Consequently, following the analysis of Corbin & Boroson (1996) we have constructed a template of the FeII emission around the MgII line from an archival IUE spectrum of the narrow line Seyfert galaxy I Zw 1. During the fitting process the amplitude and FWHM of the FeII template were left as free parameters in order to obtain the best possible match to the FeII emission of each object.

4   ESTIMATING THE BLR RADIUS

In order to provide an estimate of R_{BLR} it is necessary, in the absence of reverberation mapping, to exploit the known correlation between R_{BLR} and AGN continuum luminosity. By combining the results of their reverberation mapping observations with those of Wandel, Peterson & Malkan (1999), Kaspi et al. (2000) investigated the correlation between R_{BLR} and 5100Å continuum luminosity and found a best-fit of the form $R_{BLR} \propto \lambda L_{5100}^{0.70\pm0.03}$. In their re-analysis of the same correlation, Peterson et al. (2000) found a best fitting relation of the form $R_{BLR} \propto \lambda L_{5100}^{0.62\pm0.02}$. As well as being important within the context of the virial black-hole mass estimate, the slope of the $R_{BLR} - \lambda L_\lambda$ relation is of intrinsic interest because it provides information about the AGN ionization parameter U ($U = \frac{Q}{4\pi r^2 c}$, where $Q = \int \frac{L_\nu}{h\nu} d\nu$). For example, neither of the two fits mentioned above are consistent with the relation $R_{BLR} \propto \lambda L_\lambda^{0.5}$ expected if the ionization parameter is approximately the same for all AGN, regardless of luminosity. In this section we investigate the slope of the $R_{BLR} - \lambda L_\lambda$ relation using continuum luminosity measurements at both 3000Å and 5100Å.

4.1   Regression analysis

Given the potential influence of the $R_{BLR} - \lambda L_\lambda$ relation upon the accuracy of the virial black-hole mass estimator, we have chosen to employ three different regression techniques in our analysis to explore the possible variation in the best-fitting slope. The first technique is a straightforward weighted least-squares fit (WLS), in which the fit is weighted by the error in the reverberation mapping radius (Press et al. 1992). The second technique is a robust iterative chi-square fit (FITxy) in which the errors in both variables are taken into account (Press et al. 1992). However, although FITxy takes into account the errors on both variables, it does not account for the fact that there is likely to be intrinsic scatter in the $R_{BLR} - \lambda L_\lambda$ relation. To account for this, the third technique we have employed is the BCES estimator of Akritas & Bershady (1996) which accounts for errors in both variables and intrinsic scatter.

4.2   The radius-luminosity relation at 3000Å and 5100Å

The results of the fitting process (in $\log - \log$ space) of both the $R_{BLR} - \lambda L_{3000}$ and $R_{BLR} - \lambda L_{5100}$ relations are listed in Table 2 where the listed BCES fit is the bisector. It can be seen from Table 2 that the results of all three regression methods are consistent with each other for both the $R_{BLR} - \lambda L_{5100}$ and $R_{BLR} - \lambda L_{3000}$ relations. Furthermore, it can be seen that all three regression methods indicate that the $R_{BLR} - \lambda L_{3000}$ relation is fully consistent with a slope of $\lambda L_\lambda^{0.5}$, as expected for a constant ionization parameter.

The three fits to the $R_{BLR} - \lambda L_{5100}$ relation indicate that a slope of a $\lambda L_\lambda^{0.6}$ is more appropriate for our choice of continuum data, in good agreement with the fit of Peterson et al. (2000). This is flatter than the slope of $\lambda L_\lambda^{0.7}$ previously determined for the $R_{BLR} - \lambda L_{5100}$ relation by Kaspi et al. (2000), although the two are formally consistent.

There are two effects which are responsible for our finding of a flatter slope in the $R_{BLR} - \lambda L_{5100}$ relation.

Object	z	$\log(\lambda L_{3000})$ /W	$\log(\lambda L_{5100})$ /W	$\log(R_{BLR})$ /lt-days	MgII FWHM /kms^{-1}		Hβ FWHM /kms^{-1}	
PG 0026+129	0.142	38.23	38.07	2.05			1860	1
PG 0052+251	0.155	38.29	38.04	2.13			5200	1
PG 0804+761	0.100	38.40	37.96	2.19			3070	1
PG 0844+349	0.064	37.61	37.44	1.38	3800	2	3800	1
PG 0953+414	0.239	38.69	38.41	2.18			3130	1
PG 1211+143	0.085	38.20	38.00	2.00	2050	5	1860	1
PG 1226+023	0.158	39.23	38.97	2.59	3160	5	3520	1
PG 1229+204	0.064	37.53	37.33	1.70	2560	5	3360	1
PG 1307+085	0.155	38.26	38.01	2.09			5320	1
PG 1351+640	0.087	37.93	37.79	2.36	2790	5	5660	1
PG 1411+442	0.089	37.68	37.53	2.01	1940	5	2670	1
PG 1426+015	0.086	38.11	37.78	1.98			6820	1
PG 1613+658	0.129	37.85	37.74	1.59			8450	1
PG 1617+175	0.114	38.16	37.74	1.93			5330	1
PG 1700+518	0.292	38.75	38.70	1.94			2210	1
PG 1704+608	0.371	38.84	38.72	2.50			6560	1
PG 2130+099	0.061	37.77	37.47	2.30	4360	2	2330	1
3C 120	0.035	37.80	36.94	1.62	3360	2	1910	3
3C 390	0.052	36.49	36.89	1.36	8410	2	10000	3
Akn 120	0.035	37.60	37.22	1.57	9660	2	5800	3
F9	0.047	37.62	37.22	1.21	5680	2	6080	4
IC 4329A	0.016	34.25	36.28	0.15			5050	3
Mrk 79	0.022	36.42	36.70	1.26	4730	2	4470	3
Mrk 110	0.035	36.77	36.66	1.27	2420	2	2120	1
Mrk 335	0.026	37.15	36.87	1.21	8605	2	5685	6
Mrk 509	0.033	37.67	37.24	1.88	4790	2	2270	4
Mrk 590	0.026	36.88	36.78	1.30	4370	2	2470	3
Mrk 817	0.032	36.99	36.80	1.19	5770	2	4490	3
NGC 3783	0.009	36.32	36.31	0.65	2690	2	3780	4
NGC 3227	0.004	35.18	35.37	1.04			4920	3
NGC 4051	0.003	35.08	34.78	0.77	2790	2	1170	3
NGC 4151	0.003	34.93	35.92	0.48	3990	2	5910	3
NGC 5548	0.014	36.52	36.50	1.33	5420	2	6200	4
NGC 7469	0.017	36.95	36.81	0.69	3258	2	3000	3

Table 1. Data for the reverberation mapped sample. Columns 1 and 2 detail the name and redshift of each object. Columns 3 and 4 list the monochromatic luminosities at 3000Å and 5100Å respectively. The 3000Å and 5100Å luminosities for the PG quasars are derived from the spectrophotometric study of Neugebauer et al. (1987). For the Seyfert galaxies the 3000Å luminosities are derived from new fits to IUE archive spectra, while the 5100Å luminosities are taken from Kaspi et al. (2000) after conversion to our cosmology. Column 5 lists the BLR radius measurements from Kaspi et al. (2000), expect for NGC 4051 which is taken from Peterson et al. (2000). Columns 6 & 7 detail the FWHM of the MgII and Hβ emission lines respectively. The references for the FWHM measurements are as follows : 1. Boroson & Green (1992), 2. This work, 3. Peterson, Wandel & Malkan (1999), 4. Marziani et al. (1996), 5. Corbin & Boroson (1996) and 6. Zheng et al. (1995)

Firstly, our choice of cosmology ($\Omega_m = 0.3, \Lambda = 0.7, H_0 = 70$ kms^{-1}Mpc^{-1}) results in higher luminosities for the 17 PG quasars in the RM sample, compared to the $\Omega_m = 1$, $\Lambda = 0, H_0 = 75$ kms^{-1}Mpc^{-1} cosmology adopted by Kaspi et al., while having little effect on the luminosities of the lower redshift Seyfert galaxies. Secondly, further flattening of the slope is due to the fact that the 5100Å fluxes for the PG quasars adopted here, derived from the Neugebauer et al. (1987) data, are typically ~ 0.1 dex higher than those determined by Kaspi et al. Indeed, if we adopt the same PG quasar luminosities and cosmology as Kaspi et al., then the BCES bisector fit to the $R_{BLR} - \lambda L_{5100}$ relation becomes: $R_{BLR} \propto \lambda L_{5100}^{0.65 \pm 0.11}$, entirely consistent with the slope determined by Kaspi et al.

Throughout the remainder of the paper we adopt the BCES bisector fits as our best estimate of the $R_{BLR} - \lambda L_\lambda$ relation at both 3000Å and 5100Å . The bisector fits to both

data-sets are shown in Fig 1 and have linear versions as follows:

$$R_{BLR} = (25.2 \pm 3.0)\left[\lambda L_{3000}/10^{37}W\right]^{(0.47 \pm 0.05)} \quad (2)$$

$$R_{BLR} = (26.4 \pm 4.4)\left[\lambda L_{5100}/10^{37}W\right]^{(0.61 \pm 0.10)} \quad (3)$$

where R_{BLR} is in units of light-days.

5 ESTIMATING THE BROAD-LINE VELOCITY

After successfully calibrating the $R_{BLR} - \lambda L_{3000}$ relation, the second required element of the UV black-hole mass estimator is to calibrate the MgII FWHM as a substitute for Hβ . As discussed in Section 1, the principle reason for adopting MgII as the UV Hβ proxy is that it is a strong,
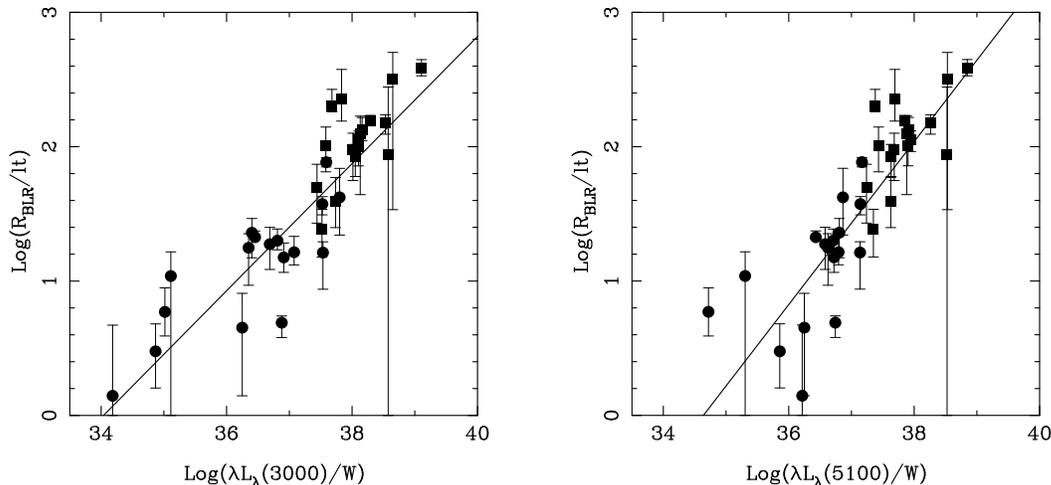
Figure 1. The correlation between broad-line radius and AGN continuum luminosity at 3000Å and 5100Å . The 17 PG quasars are shown as filled squares and the 17 Seyfert galaxies are shown as filled circles. The best-fitting BCES bisector fits to both correlations are shown as solid lines, and correspond to $R_{BLR} \propto \lambda L_{3000}^{0.47}$ and $R_{BLR} \propto \lambda L_{5100}^{0.61}$ respectively.

Method	λ	b	a
WLS	5100Å	0.57 ± 0.02	-19.53 ± 0.80
FITxy	5100Å	0.60 ± 0.02	-20.75 ± 0.92
BCES	5100Å	0.61 ± 0.10	-21.00 ± 3.67
WLS	3000Å	0.50 ± 0.02	-17.19 ± 0.70
FITxy	3000Å	0.53 ± 0.02	-18.08 ± 0.82
BCES	3000Å	0.47 ± 0.05	-16.10 ± 1.69

Table 2. Results of the regression analysis of the correlation between BLR radius and the AGN continuum luminosity at 5100Å and 3000Å . The fits were performed in $\log - \log$ space and are of the form: $\log R_{BLR} = b \log(\lambda L_\lambda) + a$. The three different regression methods are discussed in the text.

fully-permitted, low-ionization line, and as such should provide the best UV analog of Hβ . Moreover, because the ionization potentials of Hβ and MgII are very similar, the two lines should both be emitted at approximately the same radius from the central ionizing source. Fortunately, this assumption can be tested directly using the 22 objects from the RM sample for which we have MgII FWHM measurements. If MgII and Hβ are being produced at the same broad-line radius then, if the BLR is virialized, we should see a 1:1 relation between MgII FWHM and Hβ FWHM. Fig 2 shows MgII FWHM versus Hβ FWHM for the 22 objects from the RM sample with MgII FWHM measurements. The solid line in Fig 2 shows an exact 1:1 relation between MgII and Hβ FWHM. It can be seen that, with the exception of NGC 4051, the objects in the RM sample are perfectly consistent with MgII and Hβ tracing the same BLR velocity. The clear outlier, NGC 4051, is a well studied example of a narrow-line Seyfert 1 (NLS1). The Hβ FWHM for this object has been determined by numerous authors and is consistently found to be around 1000 kms^{-1} (eg. Wandel, Peterson & Malkan (1999) find Hβ FWHM=1170 kms^{-1}). However, from our line-fitting of IUE archive spectra we find

a strong broad component to the MgII emission line with FWHM=2790 kms^{-1}.

In fact, several previous studies have found that the UV emission lines of NLS1 possess strong broad components which are not seen in their Balmer lines (eg. Rodríguez-Pascual, Mas-Hesse & Santos-Lleó 1997, Zheng et al. 1995). This suggests that MgII may actually provide a better estimate of the BLR velocity of low-ionization gas in NLS1, where the Balmer lines could be biased, at least in part, by inclination effects. Irrespective of the reason why NGC 4051 is an outlier in Fig 2, we can safely exclude it from a regression fit to the MgII - Hβ FWHM relation. The reason for this is that we are principally interested in providing a UV black-hole mass estimator for high redshift quasars, the vast majority of which have Hβ FWHM > 2000 kms^{-1}. The dotted line in Fig 2 shows the BCES bisector fit which is equivalent to a relation of the form:

$$H\beta(\text{FWHM}) \propto MgII(\text{FWHM})^{1.02 \pm 0.14} \qquad (4)$$

which is clearly consistent with a linear relation. In the light of this result, an exact 1:1 relation between the MgII FWHM and Hβ FWHM is assumed in the next section for the final calibration of the UV black-hole mass estimator.

6 THE UV BLACK-HOLE MASS ESTIMATOR

Having determined in the previous two sections the $R_{BLR} - \lambda L_{3000}$ relation and the 1:1 scaling between Hβ FWHM and MgII FWHM, we are now in a position to derive our UV black-hole mass estimator. In Fig 3 we show the reverberation mapping black-hole mass estimate versus the new UV mass estimate, which uses the $R_{BLR} - \lambda L_{3000}$ relation to estimate R_{BLR} and the MgII FWHM to trace the BLR velocity. It is clear from Fig 3 that Mrk 335 is an outlier. As with NGC 4051, Mrk 335 is another example of a NLS1. The reason Mrk 335 is an outlier in Fig 3 is that the FWHM of the variable component of its Hβ line determined from reverberation mapping is only 1260 kms^{-1} (Wandel, Peterson & Malkan 1999), while from our line-fitting of IUE
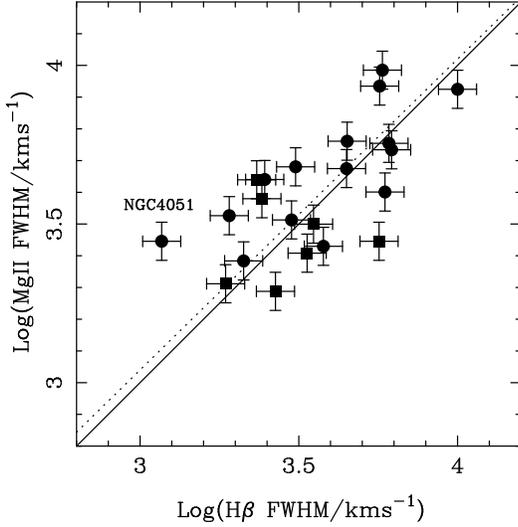
Figure 2. A Log-Log plot of MgII FWHM versus Hβ FWHM for the 22 objects from the RM sample for which it was possible to obtain measurements of both line-widths. The solid line is an exact 1:1 relation. The dotted line is the BCES bisector fit, excluding NGC 4051, and has slope of 1.02 ± 0.14. A 15% error in the FWHM of Hβ and MgII has been assumed. Symbols are as Fig 1.

archive spectra we detect a strong broad component in the MgII line with FWHM=8605 kms^{-1}. Our line-fitting results for this object are in excellent agreement with those of Zheng et al. (1995) who detected a broad MgII component of FWHM=8218 kms^{-1}. Again, as mentioned in the previous section, it appears a possibility that for at least some NLS1's the width of the Hβ emission line may not be a reliable tracer of BLR velocities. Of course, it is also possible that Mrk 335 may simply be a genuine outlier. The solid line in Fig 3 is the bisector fit to the data, excluding Mrk 335, and has the form:

$$\log M_{bh}(RM) = 1.12(\pm 0.22)\log M_{bh}(UV)$$
$$-1.08(\pm 1.75) \qquad (5)$$

again, consistent with a linear relation. Consequently, our final calibration of the UV mass estimator has the form:

$$\log M_{bh}(RM) = \log M_{bh}(UV) - 0.16 \qquad (6)$$

where the off-set of 0.16 is adopted to ensure a mean $M_{bh}(RM):M_{bh}(UV)$ ratio of unity. In terms of a useful formula the best fitting calibration of the UV black-hole mass estimator is therefore:

$$\frac{M_{bh}}{M_\odot} = 3.37 \left(\frac{\lambda L_{3000}}{10^{37}W}\right)^{0.47} \left(\frac{FWHM(MgII)}{\text{kms}^{-1}}\right)^2 \qquad (7)$$

For completeness we have also re-derived the optical (Hβ) virial black-hole mass estimator using our re-analysis of the $R_{BLR} - \lambda L_{5100}$ relation in Section 4. As expected, the correlation between $M_{bh}(RM)$ and $M_{bh}(H\beta)$ is also consistent with being linear $(M_{bh}(RM) \propto M_{bh}(H\beta)^{0.87\pm0.18})$ which, in the same fashion as for the UV estimate, leads to:

$$\frac{M_{bh}}{M_\odot} = 4.74 \left(\frac{\lambda L_{5100}}{10^{37}W}\right)^{0.61} \left(\frac{FWHM(H\beta)}{\text{kms}^{-1}}\right)^2 \qquad (8)$$
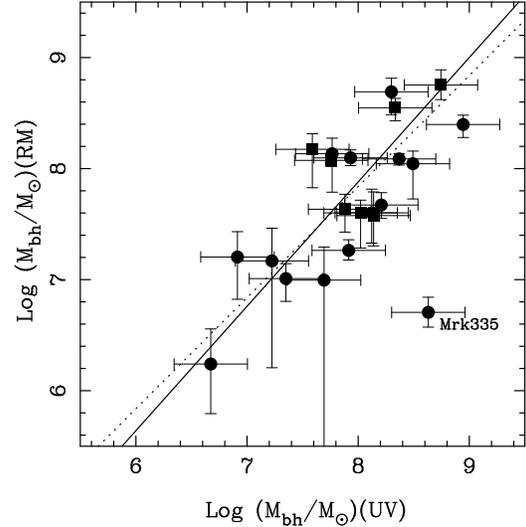
Figure 3. Full reverberation mapping black-hole mass estimate (based on R_{BLR} measurements and the rms Hβ FWHM) plotted against the UV mass estimate (based on the $R_{BLR} - \lambda L_{3000}$ relation of Eqn 2 and the FWHM of MgII) for the 22 objects from the RM sample for which it was possible to obtain MgII FWHM measurements. The solid line is the BCES bisector fit, excluding Mrk 335, which has a slope of 1.12 ± 0.22. The dotted line is the adopted linear relation (Eqn 6). Symbols as in Fig 1.

6.1 Accuracy of the UV estimator

Having arrived at the final calibration of the UV black-hole mass estimator it is of obvious interest to assess the accuracy with which it can reproduce the full reverberation mass estimate. Excluding Mrk 335, the mean difference between the reverberation and the UV estimator is :

$$< \log(M_{bh})(RM) - \log(M_{bh})(UV) >= 0.00 \pm 0.40 \qquad (9)$$

where the quoted uncertainty is the standard deviation (σ) and not the standard error. Therefore, provided the RM sample is representative of broad-line AGN in general, we conclude that the UV black-hole estimator provided by Eqn 7 can reproduce the reverberation black-hole mass to within a factor of 2.5 (1σ). For the same sample the uncertainty on the optical estimator given in Eqn 8 is a factor of 2.7.

7   APPLICATION TO QUASAR SURVEYS: THE LBQS AND MQS

Having derived the desired black-hole mass estimator in the previous section, we next assess its performance when applied to the spectra of the LBQS and the radio-selected MQS. If the new UV black-hole mass estimator is to be used in the analysis of high-redshift quasars, it is clearly important to ensure that it does not produce results which are biased with respect to the usual optical (Hβ) estimator. Therefore, our intention in this section is to simply test how the new UV mass estimator (Eqn 7) compares to the usual optical mass estimator (Eqn 8) when applied to those objects from the LBQS and MQS for which both the appropriate UV (λL_{3000}, MgII FWHM) and optical (λL_{5100}, Hβ FWHM) data are available.

Due to the fact that the LBQS is optically selected, while the MQS is a complete radio-selected quasar sample, applying the UV black-hole mass estimator to both samples allows us to ensure that Eqn 7 is equally applicable to both radio-quiet and radio-loud quasars.

7.1 The Large Bright Quasar Survey

The LBQS consists of 1058 optically-selected quasars in the redshift range $0.2 < z < 3.3$ (see Hewett, Foltz & Chaffee (1995) for a full description). A comprehensive study of the optical continuum and emission line properties of 992 quasars from the LBQS has recently been published by Forster et al. (2001). In this section we use data from Forster et al. for a 99-object sub-sample with reliable measurements of both MgII and Hβ FWHM and continuum fluxes at 3000Å and 5100Å . This sub-sample comprises 68% of the 145 LBQS objects in the redshift range $0.20 < z < 0.66$ within which both MgII and Hβ fall on the LBQS spectra.

7.2 The Molonglo quasar sample

The Molonglo quasar sample is a complete, radio-selected, sample consisting of 111 quasars in the redshift range $0.1 < z < 2.9$ with a 408 MHz flux density greater than 0.95 Jy (Kapahi et al. 1998). Optical spectra for 79 MQS quasars were published by Baker et al. (1999), together with a preliminary analysis of their emission line properties. We are currently engaged in an automated study of the optical and UV emission lines from the MQS optical spectra (kindly provided by J. Baker), from which it has been possible to reliably measure the MgII and Hβ FWHM for 29/38 objects where the MQS spectra include both emission lines. Unlike the LBQS, Baker (1997) has shown that many MQS objects display substantial reddening in their optical spectra. As a result, the continuum luminosities of the reddest MQS objects were de-reddened using the SMC extinction curve of Pei (1992), assuming an intrinsic continuum slope of $\alpha = 0.5$ ($f\nu \propto \nu^{-\alpha}$) which was found by Baker (1997) to be typical of the least reddened MQS objects.

7.3 Optical versus UV black-hole mass estimators

In Fig 4 we show the optical black-hole mass estimator plotted against the new UV black-hole mass estimator for a combined sample of 150 objects, comprising 99 from the LBQS, 29 from the MQS and the 22 objects of the RM sample. Also shown is the BCES bisector fit to the LBQS and MQS objects which has the form:

$$\log M_{bh}(H\beta) = 1.00(\pm 0.08) \log M_{bh}(MgII)$$

$$+0.06(\pm 0.67) \qquad (10)$$

which, as expected, is perfectly consistent with a linear relation. In Fig 5 we show a histogram of $\log M_{bh}(MgII) - \log M_{bh}(H\beta)$ for the 128 objects from the LBQS and MQS. The solid line shows the best-fitting gaussian which has $\sigma = 0.41$. These results, in combination with those of Section 6, lead us to conclude that compared to the traditional optical black-hole mass estimator, the new UV estimator provides results which are unbiased and of equal accuracy.
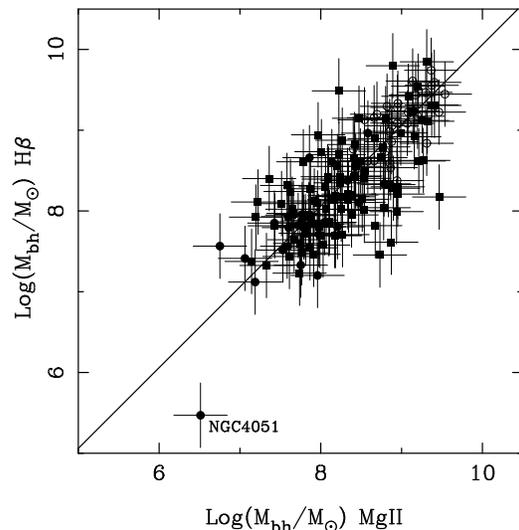
Figure 4. The optical (Hβ) versus UV (MgII) virial black-hole estimators for 150 objects from the RM (filled circles), LBQS (filled squares) and MQS (open circles) samples. The solid line is the BCES bisector fit to the 128 objects from the MQS and LBQS samples and has a slope of 1.00 ± 0.08. The outlier NGC4051 has been highlighted (see Section 5).
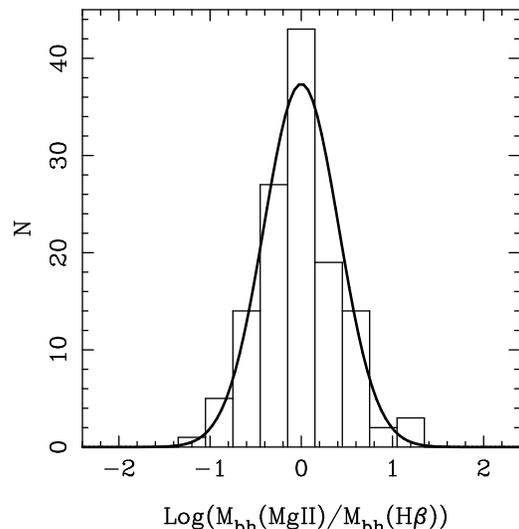
Figure 5. Histogram of $\log M_{bh}(MgII) - \log M_{bh}(H\beta)$ for the 128 objects from the LBQS and MQS shown in Fig 4. Also shown is the best-fitting gaussian which has $\sigma = 0.41$.

7.4 Black-hole mass and the radio-loudness dichotomy

Although a full analysis of the black-hole masses of the LBQS and MQS samples is beyond the scope of this paper, we will briefly comment here on one obvious feature of Fig 4. It is immediately apparent from Fig 4 that the MQS quasars are confined to the highest black-hole masses. In fact, 27/29 of the MQS quasars have black-hole masses $\geq 10^{8.5}$ M$_\odot$, adopting either the UV or optical mass estimator. In contrast, only 17% of the 99 LBQS quasars have UV and optical black-hole mass estimates which are both $\geq 10^{8.5}$ M$_\odot$. Naively this would appear to suggest that there is a clear division in black-hole mass between the radio-selected MQS

and the largely radio-quiet LBQS. However, because the wavelength coverage of the LBQS spectra only extends to $\sim$ 7500Å, compared to $\sim$ 10000Å for those of the MQS, the need to include both MgII and Hβ on the spectra introduces a considerable redshift bias into the two sub-samples under investigation here. Due to the differences in wavelength coverage the mean redshift of the LBQS sub-sample is 0.33 ± 0.01, while that of the MQS is 0.63 ± 0.03. Consequently, the members of the MQS sub-sample are on average more optically luminous than those of the LBQS sub-sample, with an average luminosity of $\log(\lambda L_{5100}/\mathrm{W}) = 38.14 \pm 0.08$ compared to $\log(\lambda L_{5100}/\mathrm{W}) = 37.64 \pm 0.07$. Therefore, with reference to the $R_{BLR} - \lambda L_\lambda$ relation, we would expect that, simply due to this luminosity bias, the average black-hole mass of the MQS sub-sample would be a factor of ~ 2 larger than that of the LBQS. However, in reality the average black-hole mass of the MQS sub-sample is $10^{9.10 \pm 0.07}\,\mathrm{M_\odot}$ whereas that of the LBQS sub-sample is more than a factor of 6 lower at $10^{8.27 \pm 0.06}\,\mathrm{M_\odot}$[*].

The origin of the additional factor of three difference in the average black-hole masses is a highly significant difference in the distributions of Hβ and MgII FWHM. For example, the average MgII FWHM of the MQS sub-sample is a factor of 1.56 ± 0.11 greater than the average MgII FWHM of the LBQS sub-sample. The equivalent factor for Hβ FWHM is 1.68 ± 0.14. The application of a Kolmogorov-Smirnov test returns a probability of $p = 1.33 \times 10^{-6}$ that the two Hβ FWHM distributions are drawn from the same parent distribution ($p = 4.1 \times 10^{-9}$ for the MgII FWHM distributions).

It is important to note that the differences in the FWHM distributions of the two samples do not appear to be related to the previously mentioned redshift/luminosity bias. An application of the partial spearman rank correlation test (Macklin 1982) reveals no significant correlations between Hβ FWHM, redshift and λL_{5100} or MgII FWHM, redshift and λL_{3000}. In fact, these results are in good agreement with previous studies of the black-hole masses of radio-quiet and radio-loud quasars which were not subject to a redshift/luminosity bias. In their study of a sample of radio-loud and radio-quiet quasars with a matched redshift-luminosity distribution at $z \lesssim 0.5$, McLure & Dunlop (2002) found the average black-hole mass of the radio-loud quasars to be a factor of $\simeq 2$ larger than their radio-quiet counterparts, albeit with a large overlap. Likewise, Laor (2000) found a clean separation in black-hole mass within the PG quasar sample, with the radio-loud quasars being confined to $M_{bh} \gtrsim 10^9\,\mathrm{M_\odot}$. In contrast, from their study of the First Bright Quasar Survey (FBQS), Lacy et al. (2001) concluded that the apparent gap in the quasar black-hole mass – radio-power plane is in fact filled by previously undetected radio-intermediate quasars.

In either case, it is clear that genuinely powerful, low-frequency selected, radio-loud quasars harbour central black-hole masses drawn from the extreme end of the AGN black-hole mass function. At present it is not clear whether the low frequency of radio-quiet quasars with $M_{bh} >$

$10^{8.5}\,\mathrm{M_\odot}$ is real or, alternatively, is due to an inclination selection effect whereby the line-widths of optically selected quasars are biased to low values by a preference for selecting objects close to the line of sight. A more detailed analysis of the black-hole masses of high redshift radio-loud and radio-quiet quasars, the correlation between black-hole mass and radio power and the evidence for the role of inclination effects will be presented in a series of forthcoming papers (McLure et al. 2002, in prep).

Finally, we note that our finding that the FWHM of Hβ and MgII in the powerful radio-selected MQS objects are exclusively restricted to $\gtrsim$ 4000 kms^{-1} is of interest in the context of recent work on the location of radio-loud and radio-quiet AGN in so-called eigenvector 1 space (Marziani et al. 2001). In their study Marziani et al. concluded that powerful radio-loud quasars appear to be restricted to Hβ FWHM > 4000 kms^{-1}, in excellent agreement with our analysis of the MQS spectra.

8 CONCLUSIONS

A new technique for estimating the central black-hole masses of high-redshift quasars using the MgII FWHM and 3000Å quasar continuum luminosity has been presented. The new technique has been calibrated using a sample of 34 low redshift AGN with black-hole mass measurements based on long-term reverberation mapping experiments. The reliability of the new technique, with respect to the established optical virial black-hole mass estimator, has been tested using published data for the LBQS together with the results of a new analysis of the emission line properties of the MQS. The main conclusions of this study can be summarized as follows:

• The correlation between R_{BLR} and monochromatic 3000Å continuum luminosity is found to display less scatter than that between R_{BLR} and 5100Å monochromatic continuum luminosity.

• The correlation between R_{BLR} and 3000Å continuum luminosity is found to be consistent with a relation of the form $R_{BLR} \propto \lambda L_\lambda^{0.5}$, as expected for a constant ionization parameter in all AGN, irrespective of luminosity

• The FWHM of MgII is found to be an effective substitute for the FWHM of Hβ . The relationship between the two FWHM is found to be perfectly consistent with an exact 1:1 scaling.

• Combining the $R_{BLR} - \lambda L_{3000}^{0.47}$ relation with the FWHM of MgII produces a virial black-hole mass estimator based on rest-frame UV observables which is capable of reproducing black-hole masses determined from reverberation mapping to within a factor of 2.5 (1σ)

• An application to objects from the LBQS and MQS demonstrates that the new UV black-hole mass estimator produces results which are unbiased, and of equal accuracy to the established optical (Hβ) black-hole mass estimator.

• We therefore conclude that the new UV black-hole mass estimator is ideal for determining quasar black-hole masses in the redshift range $0.25 < z < 2.5$ via optical spectroscopy alone.

---

[*] These figures are for the optical (Hβ) mass estimator although, as expected from Fig 4, the black-hole mass difference is comparable if the UV mass estimator is adopted ($\Delta M_{bh} = 0.71$ dex)

9   ACKNOWLEDGMENTS

REFERENCES

Akritas M.G., Bershady M.A., 1996, ApJ 470, 706
Baker J.C., 1997, MNRAS, 286, 23
Baker J.C., Hunstead R.W., Kapahi V.K., Subrahmanya C.R., 1999, ApJS, 122, 29
Barthel P.D., 1989, ApJ, 336, 606
Boroson T.A., Green R.F., 1992, ApJS, 80, 109
Brotherton M.S., ApJS, 1996, 102, 1
Corbin M.R., Boroson T.A., 1996, ApJS, 107, 69
Hewett P.C., Foltz C.B., Chaffee F.H., 1995, AJ, 109, 1498
Dunlop J.S., McLure R.J., Kukula M.J., Baum S.A., O'Dea C.P., Hughes D.H., 2002, MNRAS, submitted, astro-ph/0108397
Forster K., Green P.J, Aldcroft T.L., Vestergaard M., Foltz C.B., Hewett P.C., 2001, ApJS, 134, 35
Ferrarese L., Pogge R.W., Peterson B.M., Merritt D., Wandel A., Joseph C.L., 2001, ApJ, 555, L79
Gebhardt K., et al., 2000, ApJ, 543, L5
Kapahi V.K., Athreya R.M., Subrahmanya C.R., Baker J.C., Hunstead R.W., McCarthy P.J., van Breugel W., 1998, ApJS, 118, 327
Kaspi S., Smith P.S., Netzer H., Maoz D., Jannuzi B.T., Giveon U., 2000, ApJ, 533, 631
Krolik J.H., 2001, ApJ, 551, 72
Lacy M., Laurent-Muehleisen S.A., Ridgway S.E., Becker R.H., White R.L., 2001, ApJ, 551, L17
Laor A., 2000, ApJ, 543, L111
Laor A., 2001, ApJ, 553, 677
McLure R.J., Dunlop J.S., 2001, MNRAS, 327, 199
McLure R.J., Dunlop J.S., 2002, MNRAS, 331, 795
Macklin J.T., 1982, MNRAS, 199, 1119
Marziani P., Sulentic J.W., Dultzin-Hacyan D., Calvani M., Moles M., 1996, ApJS, 104, 37
Marziani P., Sulentic J.W., Zwitter T., Dultzin-Hacyan D., Calvani M., 2001, ApJ, 558, 553
Neugebauer G., Green R.F., Matthews K., Schmidt M., Soifer B.T., Bennett J., 1987, ApJS, 63, 615
Onken C.A., Peterson B.M., 2002, ApJ, in press, astro-ph/0202382
Pei Y.C., 1992, ApJ, 395, 130
Peterson B.M., Wandel A., 2000, ApJ, 540, L13
Peterson B.M., et al., 2000, ApJ, 542, 161
Press W.H., Teukolsky S.A., Vetterling W.T., Flannery B.P., 1992, Numerical Recipes, Cambridge University Press
Rodríguez-Pascual P., Mas-Hesse J.M., Santos-Lleó M., 1997, A&A, 327, 72
Vestergaard M., Wilkes B.J., Barthel P.D., 2000, ApJ, L103
Vestergaard M., 2002, ApJ, 571, 733
Wandel A., Peterson B.M., Malkan M.A., 1999, ApJ, 526, 579
Wills B.J., Browne I.W.A., 1986, ApJ, 302, 56
Zheng W., et al., 1995, ApJ, 444, 632